Conservation of the regulated structure of folded myosin 2 in species separated by at least 600 million years of independent evolution

Hyun Suk Jung*, Stan A. Burgess*, Neil Billington*, Melanie Colegrave†, Hitesh Patel†, Joseph M. Chalovich‡, Peter D. Chantler†, and Peter J. Knight*§

*Institute of Molecular and Cellular Biology and Astbury Centre for Structural Molecular Biology, University of Leeds, Leeds LS2 9JT, United Kingdom; †Unit of Molecular and Cellular Biology, Royal Veterinary College, University of London, Royal College Street, London NW1 0TU, United Kingdom; and ‡Department of Biochemistry and Molecular Biology, Brody School of Medicine, East Carolina University, Greenville, NC 27858-4354

Edited by Carolyn Cohen, Brandeis University, Waltham, MA, and approved February 15, 2008 (received for review August 20, 2007)

The myosin 2 family of molecular motors includes isoforms regulated in different ways. Vertebrate smooth-muscle myosin is activated by phosphorylation of the regulatory light chain, whereas scallop striated adductor-muscle myosin is activated by direct calcium binding to its essential light chain. The paired heads of inhibited molecules from myosins regulated by phosphorylation have an asymmetric arrangement with motor–motor interactions. It was unknown whether such interactions were a common motif for inactivation used in other forms of myosin-linked regulation. Using electron microscopy and single-particle image processing, we show that indistinguishable structures are indeed found in myosins and heavy meromyosins isolated from scallop striated adductor muscle and turkey gizzard smooth muscle. The similarities extend beyond the shapes of the heads and interactions between them: In both myosins, the tail folds into three segments, apparently at identical sites; all three segments are in close association outside the head region; and two segments are associated in the same way with one head in the asymmetric arrangement. Thus, these organisms, which have different regulatory mechanisms and diverged from a common ancestor >600 Myr ago, have the same quaternary structure. Conservation across such a large evolutionary distance suggests that this conformation is of fundamental functional importance.

electron microscopy | molluscan muscle | regulation | smooth muscle | image processing

The myosin 2 family not only comprises those isoforms found in muscle cells that drive muscle contraction (1) but also those responsible for intracellular movements such as cytokinesis (2) or neuronal dynamics (3). Myosin 2 forms filaments from which myosin heads interact cyclically with actin powered by ATP hydrolysis. The C-terminal halves of the two heavy chains comprising each myosin molecule associate to form the α-helical coiled-coil tail, whereas the N-terminal halves fold separately to form the two heads (4). Each head has a motor domain, containing actin and ATP-binding sites, connected to the tail by an α-helical lever stabilized by an essential light chain (ELC) and a regulatory light chain (RLC) (Fig. 1*F*). In muscles controlled through myosin-linked regulation, such as vertebrate smooth and many invertebrate striated muscles, these light chains regulate myosin ATPase activity and interaction with actin.

Myosin-linked regulation can operate by two mechanisms: direct Ca^{2+} binding or phosphorylation. Molluscan striated-muscle myosin is activated directly through Ca^{2+} binding to its ELC (5); in other invertebrate striated muscles, vertebrate smooth muscle and in nonmuscle cells, myosin 2 is activated through phosphorylation of the RLC (4). Although the light chains are vital for regulation, full inactivation by either mechanism also requires both heads and the tail (6–8).

Although scallop striated and vertebrate smooth-muscle myosins (ScM and SmM, respectively) have different regulatory mechanisms, solution studies indicate that both myosins show comparable characteristics in the inactivated state. Both have very low MgATPase rates, and single turnover experiments show that most molecules trap ADP and phosphate in their active sites (9, 10). Both myosins can form compact molecules distinct from the extended molecules found at high salt concentrations (10, 11). For SmM, electron microscopy shows that the compact conformer has the tail folded back close to the heads, and a detailed structure of the head region and the path of the folded tail have been determined (12, 13). These folded molecules share structural features with filamentous myosin in the relaxed state of *Tarantula* leg muscle (14), which is regulated by phosphorylation. Although crystal structures of ScM heads provide rich information on the structural cycle of the myosin motor (15, 16), isolated ScM heads are unregulated (6). The structure of ScM in the inhibited state has therefore not previously been determined, and it is unknown whether it shares the structural characteristics of phosphorylation-regulated myosins. Such commonality would indicate that this folded conformation has functional properties key to conservation of the off-state, given that these myosins have evolved separately for >600 Myr (17). However, existing crystal structures indicate that ScM and SmM heads differ in structure so that a common structure might not be expected. SmM has a sharp kink between the motor and lever domains in both the crystal structure and the folded conformer (12, 13, 18), whereas the ScM head is unkinked and a network of interactions stabilize the unkinked structure (19) (see Fig. 1 *F* and *G*). This would appear to prevent the two motor domains of ScM interacting in the way seen in compact SmM and relaxed *Tarantula* thick filaments. By using the two-headed fragment scallop heavy meromyosin (ScHMM), many heads were found to lie beside the proximal tail ("heads-down") when inactivated, but detailed structural analysis was not attempted (20).

Consequently, we examined ScM and ScHMM in low concentrations of Ca^{2+} to determine their inhibited structures by negative staining electron microscopy, followed by single-particle image processing. We also made a quantitative comparison to the homologous SmM and SmHMM to determine the structural relationships of the inactive states of the two regulation systems.

Author contributions: P.D.C. and P.J.K. designed research; H.S.J., M.C., and H.P. performed research; S.A.B., M.C., H.P., J.M.C., and P.D.C. contributed new reagents/analytic tools; H.S.J., S.A.B., N.B., and P.J.K. analyzed data; and H.S.J., P.D.C., and P.J.K. wrote the paper.

The authors declare no conflict of interest.

This article is a PNAS Direct Submission.

§To whom correspondence should be addressed. E-mail: p.j.knight@leeds.ac.uk.

This article contains supporting information online at www.pnas.org/cgi/content/full/0707846105/DCSupplemental.

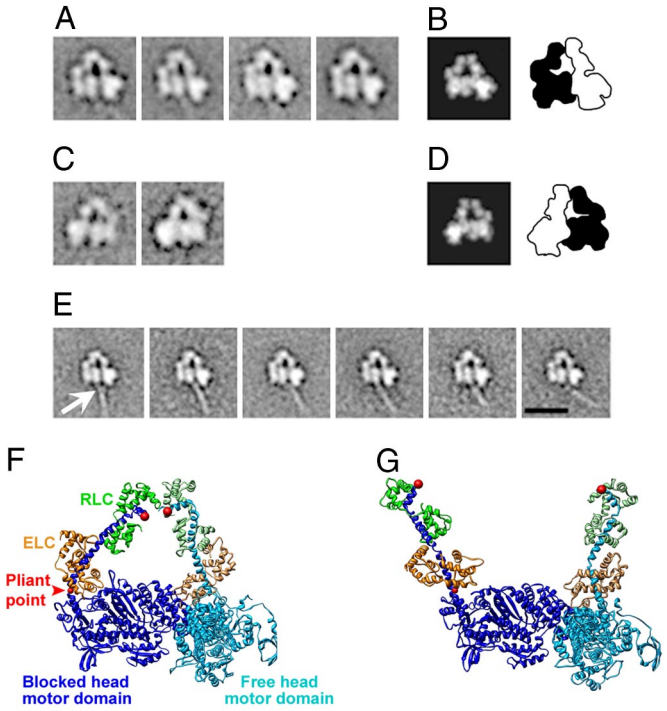

Fig. 1. Compact conformation of ScHMM. Examples of averaged images showing compact ScHMM molecules in right (*A*) and left (*C*) views, obtained from 239 and 68 compact molecules, respectively, classified by using head region features. (*B* and *D*) Corresponding projection images of the atomic model of SmHMM (12) (1i84.pdb, as modified (13) and with the tail portion removed). Adjacent cartoons show the boundary of each head in the atomic model drawn as outlines with the blocked head shaded black and the free head in white. (*E*) Averaged images from classification of the proximal part of the ScHMM tail region; white arrow points to the emergence of the tail from the head region. (*F*) Ribbon representation of *B*; heavy chains blue, ELC orange, RLC green, free head depicted in paler colors; α-carbon of Ile-792 (the ''pliant point'') in the blocked head heavy chain depicted as a sphere, colored red, and labeled; α-carbon of proline in heavy chain near the tip of each lever depicted as a red sphere. (*G*) Atomic model of two scallop myosin heads containing ADP and vanadate (1dfl.pdb), colored as in *F*; motor domains arranged by superposition on those of the SmHMM model (*F*). Note that the pliant point (Leu-778 in the scallop sequence) is unbroken α-helix, and the levers therefore diverge instead of converge. The free head shows a lesser effect of this difference in pliant-point structure, because the plane of bending is almost aligned with this direction of view. Images in *A–D*, 26.5 nm wide. (Scale bar in *E*: 20 nm.)

Results

Inhibited ScHMM and ScM Are Compact Folded Molecules. Negative staining of ScHMM and ScM [supporting information (SI) Fig. S1] shows that the heads of both can form closely apposed structures at low ionic strength and low Ca^{2+} concentration. This appearance is more common in ScM (Fig. S1*C*), suggesting that the light meromyosin segment of the tail participates in stabilizing the head arrangement. Tail regions of ScM (Fig. S1*D*) are similar in length to ScHMM (Fig. S1*B*) but stand out more, showing that the myosin tail is so compactly folded that the apposed segments appear as one structure. Single-particle image processing was used to reveal the structural detail of compact ScHMM and ScM.

Head–Head Interaction in the Inhibited Form of ScHMM. Image processing of ScHMM yields two major appearances of the heads that are related by inversion around the *y* axis (Fig. 1 *A* and *C*). Comparisons show that the two heads have a very similar shape and arrangement to those described in the atomic model of SmHMM (12) (Fig. 1 *B*, *D*, and *F*). As in SmHMM, the disposition of the ScHMM heads is asymmetric: One is a strongly bent, ''blocked'' head, and it contacts the other ''free'' head, which appears straighter in these views. Right view and left view are defined by the position of the free head.

The shape of the ScHMM blocked head shows that there must be a kink between motor and lever in the inhibited state, just as there is in SmHMM in the inhibited state (12). Unkinked ScM head structures do not create a good match to the images (Fig. 1*G*). It might be thought that the scallop molecules could form the compact structure by having a kink at a different position than the smooth-muscle ones, either within the lever or in the motor. However, it is clear from inspecting a model built by using scallop heads superposed on the SmM motor domains (Fig. 1*G*) that if there is no kink at the motor-lever junction, the ELC of the blocked head lies too peripherally to match the observed structure. It might also be thought that the wide separation of the tips of the scallop levers depicted in Fig. 1*G* might be reversed by substituting the more strongly bent chicken S1 lever that was found to be the better fit to the compact SmHMM head structure (12). We found by model building that the substitution did indeed reduce the separation of the α-carbons of the proline residues at the C terminus of the heavy chains from 12.3 nm (as in Fig. 1*G*) to 8.6 nm, but this is still a much wider separation than in the compact structure (2.5 nm; Fig. 1*F*), so would require even more bending to unite the levers at the head–tail junction as observed. Moreover, the two subdomains of each light chain in the lever are very similarly arranged in our images of the compact head structures of ScM and SmM (see below), so there is no evidence for a difference in bending within the lever between the two myosins. Inspection of the current suite of scallop/squid S1 crystal structures does not suggest an easy rearrangement within the motor domain that would allow an unkinked lever to emerge at the right site and with the right orientation to replicate the head and lever structure we see. In addition, the lever of the Ca^{2+}-free squid S1 structure (16) has a very similar shape to that of the Ca^{2+}-loaded scallop S1 structures. Therefore, the evidence is strong that ScM in this shutdown conformation has a kink at the pliant point very similar to SmM. This is a previously uncharacterized conformation of Ca^{2+}-regulated myosin.

The tail of ScHMM is flexible (Fig. 1*E*), as described for SmHMM (13). As with SmHMM, the tail emerges from the head region near the interface of the blocked and free heads (arrow in Fig. 1*E*).

Structure of the Inhibited Form of Intact ScM. Like ScHMM, averaged images of folded ScM show both right and left views (Fig. 2 *A* and *B*). The shape and arrangement of myosin heads in each view are very similar to ScHMM (Fig. 1), and the differences between classes are in staining rather than structure. Additional features in the head region of ScM derive from the folded tail. First, the tail emerges at the same location from the blocked head as in ScHMM but is broader because it is three coiled coils, not one. Second, a prominent pale spot beside the blocked head lever in ScM (Fig. 2, arrowhead) connects with a strand beside the motor domain and a strand that runs into the RLC. These connections are more clearly seen by subtracting a ScHMM averaged image from the ScM averaged image to reveal the tail (Fig. 2 *C* and *D*). The prominent spot is seen to be a sharp bend in the tail. It is also clear that no part of the tail is associated with the free head. All of these features of ScM echo those of SmM (13) and suggest that both myosins share a common inhibited structure despite their different mechanisms of control.

Regulated Myosins Fold Indistinguishably Irrespective of Control Mechanism. To test whether the two myosins adopt the same inhibited structure, new datasets of folded SmM and SmHMM were combined with the scallop data for analysis. Unlike our previous study (13), left views as well as right views of SmM were

BIOPHYSICS

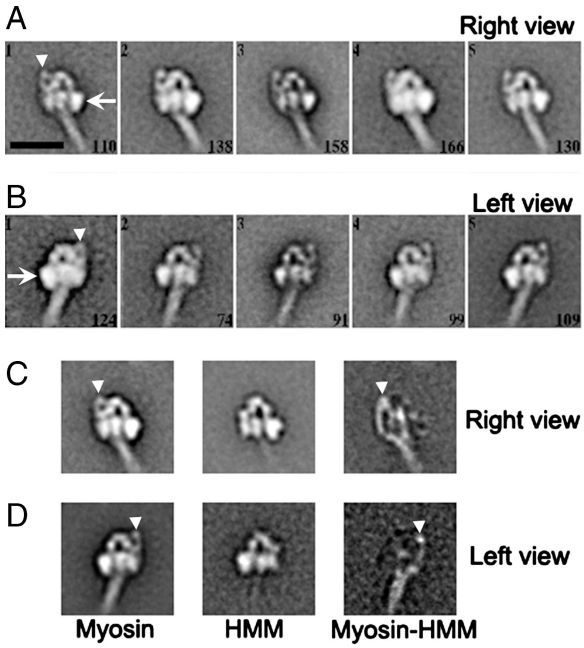

Fig. 2. Structure of folded ScM. (*A* and *B*) Averaged images of the compact conformation of ScM showing right and left views, respectively. The arrow indicates the free-head motor domain and the arrowhead indicates the prominent spot beside the blocked-head lever domain. (*C* and *D*) Image subtractions to reveal the path of the folded tail in the head region in right and left views, respectively. Arrowheads in left and right panels indicate the second bend in the tail. (*Left*) ScM averages (averaged from 702 and 497 molecules, respectively). (*Center*) Coaligned compact ScHMM averages (averaged from 239 and 68 molecules, respectively). (*Right*) ScHMM average subtracted from ScM average. Class numbers and the number of images combined in each average in *A* and *B* are shown in the upper left and lower right of each panel, respectively. (Scale bar in *A*: 20 nm.)

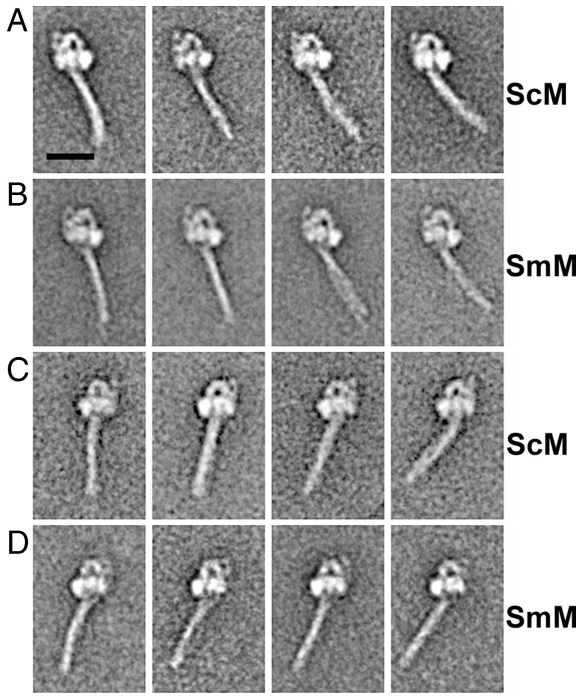

Fig. 4. Folding and flexibility of the tail in regulated myosins. (*A* and *C*) Representative averaged images of ScM in right and left views, respectively. (*B* and *D*) Averaged images of SmM comparable with those seen in *A* and *B*. (Scale bar in *A*: 20 nm.) See also Movies S1–S4.

frequent, allowing comparison with both views of ScM. However, only right views of SmHMM were seen. Global averages of the head regions of the scallop proteins (Fig. 3 *A*, *D*, and *G*) demonstrate a striking similarity with those of the smooth (Fig. 3 *C*, *F*, and *I*). The second bend in the tail is consistently observed in the same location (beside the blocked head RLC) in both myosins. The grouped myosin tail segments consistently emerge from the same part of the blocked-head motor domain and are angled either to the right or the left, in right and left views, respectively, such that the tail axis always extrapolates across the blocked head to the second bend (Fig. 4).

To compare the structural details in the head regions objectively, we combined equal numbers of ScM and SmM (or

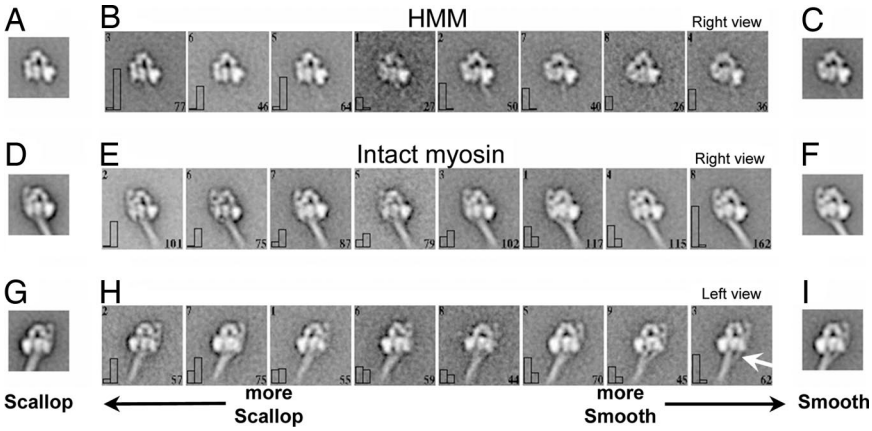

Fig. 3. Comparison of the compact conformations of ScM and SmM. (*A* and *C*) Averaged right-view images of ScHMM (*A*) and SmHMM (*C*) (183 images of each). (*D* and *F*) Averaged right-view images of ScM (*D*) and SmM (*F*) (491 images of each). (*G* and *I*) Averaged left-view images of ScM (*G*) and SmM (*I*) (303 images of each). (*B*) The right-view images of ScHMM and SmHMM were grouped together, aligned, and classified by using head-region features into eight classes. These are ranked in order of increasing proportion of SmHMM images. (*E* and *H*) Right- and left-view images of ScM and SmM treated similarly. Histogram in lower left of each image within the montages (*B*, *E*, and *H*) shows the number of SmHMM or SmM (left bar) and ScM or ScHMM (right bar) images ascribed to each class. Arbitrary class number and number of images contributing to each average are shown in the upper left and lower right corners of each image, respectively. The white arrow in *H* points to the separated region of the tail seen principally in SmM images. Images in *A*, *C*, *D*, *F*, *G*, and *I* are 31.8 nm wide; *B*, *E*, and *H* are 42.4 nm wide.

ScHMM and SmHMM) images in a given view, coaligned and coclassified them, and then ordered the eight classes according to the fraction of scallop images in the class (Fig. 3 *B*, *E*, and *H*). The classes appear remarkably similar to one another, confirming the close conformational similarities of ScM and SmM in the inhibited state. In general classes contain both species of myosin, but subtle differences between the ScM and SmM datasets give rise to strongly biased classes at either extreme of the ranking. In right views of intact molecules (Fig. 3*E*) biases arise from variation in staining rather than true structural differences. In left views of intact molecules (Fig. 3*H*) a separated region of the tail close to the blocked head is seen in some averages dominated by SmM (white arrow in Fig. 3*H*) but not in the averages dominated by ScM. ScHMM appears slightly narrower than SmHMM (compare Fig. 3*A* with 3*C*), and this is sufficient to produce almost complete segregation (Fig. 3*B*). This difference in shape is not apparent between the two myosins, so it probably arises from a slight difference in orientation of the two HMM species on the EM grid. Apart from these minor differences, the head regions of inhibited ScM and SmM were indistinguishable in both left and right views. Although there must be differences between the high-resolution structure of the two myosins, these direct comparisons confirm that the head shapes of inhibited ScM and SmM are essentially the same.

Structural comparison of the folded tail outside the head region indicates that it comprises three segments in both myosins, but unlike our previous study (13) the three segments are usually closely grouped throughout their length rather than side by side. This may be because we used sodium acetate here rather than the more chaotropic KCl. The appearance contrasts with the open, looped appearance seen by shadowing, probably because of raised salt concentrations during drying in that method (13). The folded tail is flexible (Fig. 4, and Movies S1–S4). The movies are made by arranging class averages from a classification based on features in the tail region, in order of the angle the tail makes to the head region. The second half of each movie comprises the same frames as seen in the first half but in reverse order. Note that this sequence is to illustrate the range of fleximers present: We do not suppose that the tail makes pendulum-like motions in solution. The extent of flexibility appears the same in left and right views and is less than the single coiled coil of HMM (Fig. 1*E*), indicating there are interactions between the tail segments that stiffen the tripartite tail region against thermal fluctuations. No differences are apparent between ScM and SmM folded tails, indicating that the sites of folding are also conserved and therefore that homologous regions of the tail will be in contact with the heads in both myosins.

Discussion

Head–Head Interaction in the Off State. Our images give direct evidence that the Ca^{2+}-regulated ScM and ScHMM can adopt an asymmetric motor–motor interaction in the inhibited state, as previously shown for the phosphorylation-regulated molecules of SmM and SmHMM (12, 13). Thus, such motor–motor interaction is a common motif for both myosin types regardless of sequence differences, including those within the tail. This feature of the two different regulatory mechanisms transcends the arrangement of myosin molecules within their respective thick filaments: bipolar in scallop striated adductor muscle and side-polar in vertebrate smooth muscle (21). Just as both forms of regulatory myosin possess similar cycling mechanisms defining their motor activities, these head–head interactions create a further unifying principle for inactivation of their functional properties.

The heads of Ca^{2+}-free scallop myosin have heretofore not been imaged in sufficient detail to see the relationship within the head of the two light chains to each other and the motor domain and their arrangement across the head–tail junction in the inhibited state. Although the resolution of these negative-stained images is ≈2 nm [the same as the cryo-3D structures of SmM (22) and SmHMM (12)], the error in locating the centers of domains is considerably less than this [as also exemplified by the FIONA technique (23), which detects nanometer movements from images with micrometer resolution]. We have shown by coalignment and coclassification of ScHMM with SmHMM or ScM with SmM, that the shapes of the scallop proteins are indistinguishable from the smooth-muscle ones at the current resolution. Thus, it is clear, for instance, that the relation of the ELC N-lobe to the motor domain in the blocked head matches the SmM ADP·AlF_4 structure (18) but not the ScM ADP·Vi structure (15) (Fig. 1*A* compared with *F* and *G*). The implication is that the heavy chain α-helix of ScM is disrupted at the converter–lever junction, like in SmM and unlike any crystal structure of isolated scallop heads. This is unexpected, because interactions in the ScM structure stabilize the unbroken heavy-chain α-helix (19). However, SmM heads attached to actin have an unbroken heavy chain α-helix (24), so there is a precedent for conformational switching in this section of α-helix. The close similarity of the folded state of the scallop and smooth-muscle proteins implies that the lever shape of the compact ScM and ScHMM resembles the chicken skeletal-muscle myosin lever rather than the straighter lever of scallop myosin-head structures, because the latter was reported to be a poor fit to SmM and SmHMM 3D structures (12, 22).

The bend between motor and lever that is implied by our images of inhibited ScHMM and ScM allows contact between the ELC C-lobe and "loop 1" of the motor similar to that described in the SmM ADP.AlF_4 structure (18). It remains to be established whether these interactions are a vital part of the inhibitory regulatory signal pathway, for instance by stabilizing retention of the ADP·phosphate complex in the active site and maintaining weak actin binding.

Head–Tail Interactions in the Off State. The resolution of our images does not allow atomic detail to be seen; nevertheless we may suggest some interactions between the heads and the three segments of the twice-folded tail that might stabilize the off state of the motors. In relaxed *Tarantula* thick filaments, the blocked-head motor domain makes contact with the proximal part of the tail, and it was suggested that this was an important part of the regulatory mechanism (14). Our images of ScHMM resemble this structure, which suggests that this part of the regulatory mechanism may also operate in scallop thick filaments. Segment 2 of the folded tail runs around the margin of the blocked head, which may stabilize the sharp bend between motor and lever and thereby contribute to the very low ATPase of folded ScM molecules (10). Segment 3 of the tail crosses the blocked head, where its position may be stabilized by interactions with the RLC and the motor domain, but its relationship to segment 1 of the tail is unclear. The close apposition of the three segments of the tail outside the head region suggests that there are significant interactions between them, which in turn could stabilize the conformation of the head region of the whole molecule with a folded tail. The absence of such factors may explain the lower stability we found for the compact ScHMM conformation.

Role of the Folded Myosin Conformation. Subtraction images show that segments 2 and 3 of the tail interact only with the blocked head in both ScM and SmM. Nevertheless this interaction plays a critical role in trapping the ADP·phosphate complex in the active sites of both heads, because the complex is not as well trapped in the HMM fragments (9, 10).

Although it is clear that the inhibited state is critical to regulatory myosin function *in vivo*, the role of the folded, compact molecules remains controversial. Although SmM is

organized as antiparallel side-polar filaments (21) that persist in the relaxed state, evidence is accumulating for a pool of unpolymerized myosin, presumably folded, at least in some muscles (25). In contrast, ScM remains as stable myosin filaments in relaxed striated adductor muscle (26), even though it can form a folded conformation *in vitro*. Therefore, the functional role of the folded conformation may not be related to the regulation of contractile activity in these muscles. Nevertheless, trapping of the ADP·phosphate complex is shared by these very similar structures, suggesting that this folded form may be of functional importance in the cell. One function for folded myosin could be as a transport form for newly synthesized myosin during transfer from the ribosome to the thick filaments, as postulated earlier (10), but evidence for this is still lacking.

Sequence analysis shows that SmM is closely allied to the nonmuscle branch of the myosin 2 family rather than the striated-muscle myosins. This divergence must have preceded the emergence of bilaterian phyla that occurred ≈600 Myr ago (17). Nevertheless, our data reveal that the motor–motor interaction, previously observed in unphosphorylated myosin heads in SmM and *Tarantula* myosins, is also present in the inhibited state of ScM and ScHMM, which operate by a different control mechanism, namely Ca^{2+}-dependent regulation. Moreover, the tails of full-length ScM and SmM in the inactive state adopt folded structures that are indistinguishable by our technique. Given the large evolutionary distance since divergence, two important conclusions emerge. First, the asymmetric interaction between the motors in the inhibited state is an ancient trait that must be important to successful function, regardless of the mechanism of regulatory control. Second, the folding of the tail and its specific association with the blocked head plays some vital role for myosins even where they function as unfolded molecules within stable thick filaments.

Materials and Methods

Proteins. ScM was prepared from *Pecten maximus* as described (27) with modifications (28). ScHMM was prepared as described (6) with additional modifications (20, 29). The procedures are outlined in *SI Materials and Methods*. These proteins were solubilized in 0.5 M KCl, 2 mM $MgCl_2$, 3 mM NaN_3, 10 μM $CaCl_2$, 20 mM Tris·HCl (pH 7.6). Dephosphorylated SmM and SmHMM were prepared from turkey gizzard as described (13) and stored in a solution containing 0.5 M KCl, 2 mM EGTA, 0.1 mM $MgCl_2$, 0.1 mM DTT, 10 mM imidazole·HCl (pH 7.0). These proteins were frozen dropwise in liquid N_2 and stored at −196°C.

Specimen Preparation and Electron Microscopy. Thawed myosin was first diluted with a high-salt–ATP buffer [0.5 M sodium acetate or KCl, 1 mM EGTA, 2 mM $MgCl_2$, 10 mM Mops, 0.5 mM ATP (pH 7.5 at room temperature), and the mixture was further diluted with a low-salt buffer [150 mM sodium acetate or KCl, 1 mM EGTA, 2 mM $MgCl_2$, 10 mM Mops (pH7.5 at room temperature) to give a final concentration of 10–20 nM myosin, 175 mM salt, and 25 μM ATP. HMM was diluted with the high salt–ATP buffer and further diluted to 10–20 nM with a low-salt buffer containing 20 mM sodium acetate instead of 150 mM, to give a final concentration of 35 mM sodium acetate. Carbon filmed EM grids were pretreated with UV light, 5 μl of protein solution were applied and immediately negatively stained with 1% uranyl acetate (30). Micrographs were recorded after brief observation at a nominal magnification of ×40,000 using a Jeol 1200EX microscope at 80 kV. Magnification was calibrated by using the 14.4 nm repeat of paramyosin filaments.

Image Processing. Molecules showing clear head and tail regions were selected and imported into the SPIDER suite of software for further processing (30) (see *SI Materials and Methods* for detail). An initial classification into many classes allowed the compactly folded molecules seen in left and right views to be selected from among others that were either side views, not compact, or poorly stained. These two views were then further analyzed.

ACKNOWLEDGMENTS. We thank Drs. Christine Cremo and Kevin Facemyer for stimulating discussions, Dr. Gerald Offer for producing an atomic model of the SmM coiled coil, and Mr. Michael Vy-Freedman for assistance in preparing smooth-muscle proteins. This work was supported in part by a Biotechnology and Biological Sciences Research Council (U.K.) grant (to P.D.C.) and National Institutes of Health Grant AR35216 (to J.M.C.).

1. Craig R, Padrón R (2004) in *Myology*, eds Engel AG, Franzini-Armstrong C (McGraw-Hill, New York), Vol 1, pp 129–166.
2. Robinson DN, Spudich JA (2004) Mechanics and regulation of cytokinesis. *Curr Opin Cell Biol* 16:182–188.
3. Chantler PD, Wylie SR (2003) Elucidation of the separate roles of myosins IIA and IIB during neurite outgrowth, adhesion and retraction. *IEE Proc Nanobiotechnol* 150:111–125.
4. Sellers JR (1999) *Myosins* (Oxford Univ Press, Oxford).
5. Houdusse A, Cohen C (1996) Structure of the regulatory domain of scallop myosin at 2 Å resolution: Implications for regulation. *Structure (London)* 4:21–32.
6. Kalabokis VN, Szent-Györgyi AG (1997) Cooperativity and regulation of scallop myosin and myosin fragments. *Biochemistry* 36:15834–15840.
7. Cremo CR, Sellers JR, Facemyer KC (1995) Two heads are required for phosphorylation-dependent regulation of smooth muscle myosin. *J Biol Chem* 270:2171–2175.
8. Trybus KM, Freyzon Y, Faust LZ, Sweeney HL (1997) Spare the rod, spoil the regulation: Necessity for a myosin rod. *Proc Natl Acad Sci USA* 94:48–52.
9. Cross RA, Jackson AP, Citi S, Kendrick-Jones J, Bagshaw CR (1988) Active site trapping of nucleotide by smooth and non-muscle myosins. *J Mol Biol* 203:173–181.
10. Ankrett RJ, Rowe AJ, Cross RA, Kendrick-Jones J, Bagshaw CR (1991) A folded (10 S) conformer of myosin from a striated muscle and its implications for regulation of ATPase activity. *J Mol Biol* 217:323–335.
11. Trybus KM, Huiatt TW, Lowey S (1982) A bent monomeric conformation of myosin from smooth muscle. *Proc Natl Acad Sci USA* 79:6151–6155.
12. Wendt T, Taylor D, Trybus KM, Taylor K (2001) Three-dimensional image reconstruction of dephosphorylated smooth muscle heavy meromyosin reveals asymmetry in the interaction between myosin heads and placement of subfragment 2. *Proc Natl Acad Sci USA* 98:4361–4366.
13. Burgess SA, *et al.* (2007) Structures of smooth muscle myosin and heavy meromyosin in the folded, shutdown state. *J Mol Biol* 372:1165–1178.
14. Woodhead JL, *et al.* (2005) Atomic model of a myosin filament in the relaxed state. *Nature* 436:1195–1199.
15. Houdusse A, Szent-Györgyi AG, Cohen C (2000) Three conformational states of scallop myosin S1. *Proc Natl Acad Sci USA* 97:11238–11243.
16. Yang YT, *et al.* (2007) Rigor-like structures from muscle myosins reveal key mechanical elements in the transduction pathways of this allosteric motor. *Structure (London)* 15:553–564.
17. Peterson KJ, *et al.* (2004) Estimating metazoan divergence times with a molecular clock. *Proc Natl Acad Sci USA* 101:6536–6541.
18. Dominguez R, Freyzon Y, Trybus KM, Cohen C (1998) Crystal structure of a vertebrate smooth muscle myosin motor domain and its complex with the essential light chain: Visualization of the pre-power stroke state. *Cell* 94:559–571.
19. Gourinath S, *et al.* (2003) Crystal structure of scallop myosin S1 in the pre-power stroke state to 2.6 Å resolution: Flexibility and function in the head. *Structure (London)* 11:1621–1627.
20. Stafford WF, *et al.* (2001) Calcium-dependent structural changes in scallop heavy meromyosin. *J Mol Biol* 307:137–147.
21. Craig R, Woodhead JL (2006) Structure and function of myosin filaments. *Curr Opin Struct Biol* 16:204–212.
22. Liu J, Wendt T, Taylor D, Taylor K (2003) Refined model of the 10 S conformation of smooth muscle myosin by cryo-electron microscopy 3D image reconstruction. *J Mol Biol* 329:963–972.
23. Yildiz A, *et al.* (2003) Myosin V walks hand-over-hand: Single fluorophore imaging with 1.5-nm localization. *Science* 300:2061–2065.
24. Whittaker M, *et al.* (1995) A 35-Å movement of smooth muscle myosin on ADP release. *Nature* 378:748–751.
25. Seow CY (2005) Myosin filament assembly in an ever-changing myofilament lattice of smooth muscle. *Am J Physiol* 289:C1363–C1368.
26. Millman BM, Bennett PM (1976) Structure of the cross-striated adductor muscle of the scallop. *J Mol Biol* 103:439–467.
27. Chantler PD, Szent-Györgyi AG (1978) Spectroscopic studies on invertebrate myosins and light chains. *Biochemistry* 17:5440–5448.
28. Patel H, Margossian SS, Chantler PD (2000) Locking regulatory myosin in the off-state with trifluoperazine. *J Biol Chem* 275:4880–4888.
29. Azzu V, *et al.* (2006) Calcium regulates scallop muscle by changing myosin flexibility. *Eur Biophys J* 35:302–312.
30. Burgess SA, Walker ML, Thirumurugan K, Trinick J, Knight PJ (2004) Use of negative stain and single-particle image processing to explore dynamic properties of flexible macromolecules. *J Struct Biol* 147:247–258.